Introduction, Characterization and Efficiency Optimization of a Heterojunction Solar Cell with GaAs as Back Surface Field (BSF) Layer Using ADEPT/F

A Thesis Presented to
The Academic Faculty

By

Ashiq Ibn Aziz (Student ID: 112458)
Sakibul Hasan (Student ID: 112477)
Sidratul Muntaha (Student ID: 112446)
Ahmed Noman (Student ID: 112444)

In Partial Fulfilment of Requirement for the Degree of Bachelor of Science in Electrical and Electronic Engineering

Approved By

PROF. DR. MD. ASHRAFUL HOQUE
DEPARTMENT OF ELECTRICAL AND ELECTRONIC ENGINEERING (EEE)
ISLAMIC UNIVERSITY OF TECHNOLOGY (IUT)
November, 2015

Introduction, Characterization and Efficiency Optimization of a Heterojunction Solar Cell with GaAs as Back Surface Field (BSF) Layer Using ADEPT/F

Ashiq Ibn Aziz
Student ID : 112458
(Author)

Sakibul Hasan
Student ID : 112477
(Author)

Sidratul Muntaha
Student ID : 112446
(Author)

Ahmed Noman
Student ID : 112444
(Author)

Prof. Dr. Md. Ashraful Hoque
Professor
Dept. of EEE, IUT
Supervisor

Prof. Dr. Md. Shahid Ullah
Professor
Head of the Department
EEE, IUT

Table of Contents

List of Figures

List of Tables

Introduction, Characterization and Efficiency Optimization of a Heterojunction Solar Cell with GaAs as Back Surface Field (BSF) layer Using ADEPT/F

Abstract

Energy is convertible from one form to another. So, energy conversion efficiency is a major issue for photovoltaic cells today. Researchers are continuously trying to improve the efficiency level of photovoltaic devices by introducing new materials and advanced concepts. The target is to reach a high efficiency level within affordable cost, which will lead to a mass generation of electricity using photovoltaic devices.

In this work, a III-V heterojunction solar cell has been introduced and characterized, which uses an AlGaAs heterojunction as the working p-n junction. ADEPT/F, a 1D simulation software, was used throughout the whole work for the simulation of light J-V characteristics for different designs. Energy conversion efficiency for each design was calculated from its corresponding light J-V characteristics curve. An illumination level of 1000 W/m2 (AM1.5G standard) and a concentration level of 1 sun was considered for all the simulations in the work. The photovoltaic cell has an n-on-p structure,where the p-type AlGaAs layer acts as a base, and the n-type ZnS layer serves as the emitter. The base thickness was kept at 1μm. Germanium (Ge) substrate (p-doped) was used for the structure.

Considering the high fabrication cost of III-V solar cells, a thin film solar cell design was proposed,which is only 2 μm thick (excluding the substrate thickness), and yields an efficiency of 12.16%.This efficiency was raised to 13.84% by using InP substrate, instead of Ge.

We used ADEPT software for simulating J-V curve. From the curves, we got Open circuit voltage Voc and short circuit current Isc . Then, from these, Fill Factor and efficiency were calculated.

Acknowledgements

We are grateful to our thesis supervisor, Prof. Dr. Md. Ashraful Hoque, for his continuous guidance and motivation in completing our thesis. His constant demand for making the work more elaborate finally resulted in satisfactory and successful outcomes. We would like to thank our co-supervisor K. A. S. M. Ehteshamul Haque, ex- lecturer of the Department of Electrical and Electronics Engineering, Islamic University of Technology, for providing us with necessary information about hetero-junction solar cells and for offering us a helpful introduction to ADEPT.

Symbols & Abbreviations

I	Current (A)
I_L	Photocurrent (A)
I_F	Forward current (A)
I_S	Saturation current (A)
n	Ideality factor
k	Boltzmann constant (JK^{-1})
T	Absolute temperature (K)
q	Charge of an electron (C)
I_{sc}	Short-circuit current (A)
V_{oc}	Open-circuit voltage (V)
P_m	Maximum output power (W)
V_m	Voltage at maximum power point (V)
I_m	Current at maximum power point (A)
FF	Fill Factor
V_{ocn}	Normalized open-circuit voltage (V)
η	Energy conversion efficiency (%)
E	Solar irradiance (W/cm^2)
A	Area of the solar cell (cm^2)
J_{sc}	Short-circuit current density (A/cm^2)

Chapter 1- Introduction

1.1 Solar Cells

1.1.1 History

Solar cells are semiconductor devices which convert incident light into electricity by the absorption of photons and subsequent generation of electron-hole pairs. This effect of electricity generation from light absorption, which is known as the photovoltaic effect, was first observed by the French physicist A. E. Becquerel in 1839 [1]. The first solid-state photovoltaic cell was built many years later, by Charles Fritts, in 1883. He coated Selenium (Se) with an extremely thin layer of gold to form the junction. The photovoltaic device was less than 1% efficient [2]. The first practical photovoltaic cell was developed in 1954 at Bell Laboratories [3] by the three scientists- Daryl Chapin, Calvin Souther Fuller and Gerald Pearson. They used a diffused Silicon p-n junction that achieved 6% efficiency.

At present, solar cells are built with many different technologies, and the efficiency level that these devices can achieve is pretty good. In today's world, we have bulk Si solar cells, we have thin film solar cells fabricated from Si or CdTe, we have dye-sensitized solar cells, and so on. There are even more advanced concept solar cells like Quantum Dot (QD) solar cells, hot carrier solar cells etc. Today, solar cells are used for mass generation of electricity. The added advantage of solar power plants is that they require minimum maintenance, and the input energy is clean and free.

1.1.2 Principle of Operation

Figure 1.1 presents a simplified diagram [4] of a solar cell that utilizes a single p-n junction. With no voltage applied to this junction, an electric field exists in the depletion region of the p-n junction. For simplicity, we consider that a resistive load is connected with the device. Now, photons incident on the device can create electron-hole pairs in the space-charge region, which are forcibly swept out of the depletion region by the built-in electric field, as the depletion region must be depleted of free charges. This swept out carriers produce a photocurrent IL, in the reverse-bias direction for the p-n junction. Now, the photocurrent IL produces a voltage drop across the resistive load, which forward biases the p-n junction. This forward bias produces a forward current, IF, in the forward-bias direction for the p-n junction. The net current, I, in the reverse bias direction for the p-n junction, is given by equation (1).

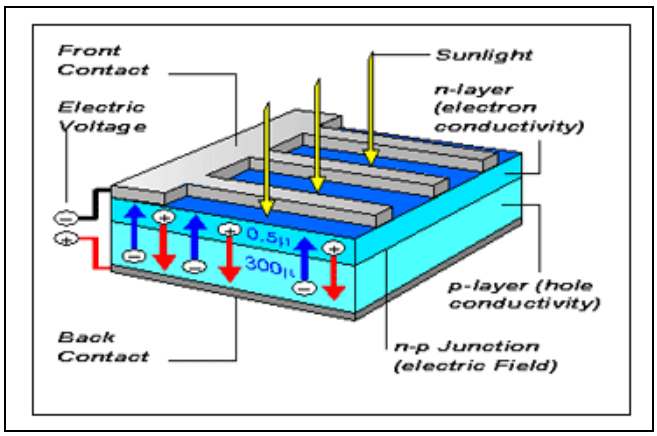

Fig. 1.1 Schematic diagram of a simplified back contact solar cell (image courtesy: ECN, the Netherlands).

$$I = IL - IF = IL - IS\,[exp\,(qV / nkT) - 1] \text{ ---------- (1)}$$

Where,

n = Ideality factor (taken as 1)
k = Boltzmann constant
T = Temperature in K
q = charge of an electron
IS = saturation current

1.1.3 Important Quantities

Now, there are two quantities of practical interest, the short-circuit current (Isc) and the open-circuit voltage (Voc). The short-circuit condition occurs when the resistive load is zero, so that V= 0. In this case, IF is zero, and the short-circuit current, Isc, is given by equation (2).

$$Isc = IL \text{ ---------- (2)}$$

Open-circuit condition occurs when the load resistance is infinity. The net current is zero in this case, which finally gives the expression of the open-circuit voltage, Voc, as shown in equation (3).

$$Voc = (nkT / q)\,ln\,(1 + (IL / IS)) \text{ ---------- (3)}$$

It is to be noted that at both short-circuit and open-circuit condition, the power output of a solar cell is zero. Actually, there is a maximum power point on the I-V characteristics graph of a solar cell where $dP/dV = 0$ (*P* is the output power). This point is called the maximum power point. The maximum outputpower, Pm, is given by,

$$Pm = VmIm \text{ ---------- (4)}$$

Where,

Vm= Voltage at Maximum Power Point
Im= Current at Maximum Power Point

Now, a quantity, termed as 'Fill Factor', is used to measure the 'squareness' of the I-V curve of a solar cell. This is the ratio of the maximum output power, Pm, to the product of short-circuit current (Isc) and the open-circuit voltage (Voc). Fill factor is commonly abbreviated as FF. A higher FF is desirable, since it increases the maximum output power.

The theoretical FF from a solar cell can be determined by differentiating the power from a solar cell with respect to the voltage and finding the voltage value for which the derivative equals to zero. This is the voltage corresponding to the maximum power point, which is denoted by Vm. An equation involving Vm is given in (5).

$$Vm = Voc - [(nkT / q) \times [\ln (qVm / nkT) + 1] \text{ ---------- (5)}$$

Solving equation (5) by iteration gives the value of Vm. Now, determining the value of Imrequires the knowledge of IL and IS. So, this method does not give a closed form solution for determining the maximum output power Pm, the knowledge of which is required for determining FF. So, for all the simulations in our work, we have used the formula [5] given by equation (6) for the calculation of FF.

$$FF = \frac{Vocn - \ln(Vocn + 0.72)}{Vocn + 1} \text{ ---------- (6)}$$

Where,

$$Vocn = \left(\frac{q}{nkT}\right) \text{Voc ---------- (7)}$$

Here,

Voc = Open-circuit voltage (in Volt)
n= Ideality factor
q= Charge of an electron = 1.6×10^{-19} Coulomb
k= Boltzmann constant
T= Temperature in K

For all the simulations, we have considered n=1, and T = 300K.

The energy conversion efficiency of a solar cell, η, is given in (8).

$$\eta = \frac{Voc \times Isc \times FF}{E \times A} \times 100\% \text{ ---------- (8)}$$

Here,
Voc = Open-circuit voltage (in Volts)
Isc = Short-circuit current (in Amperes)
FF = Fill Factor
E = Solar irradiance (in W/cm2)
A= Area of the solar cell (in cm2)

Now, Isc /A can be termed as Jsc, which is the short-circuit current density (in A/cm2). So, equation (8) can
be rewritten as,

$$\eta = \frac{Voc \times Jsc \times FF}{E} \times 100\% \text{ ---------- (9)}$$

Where,
Jsc = Short-circuit current density (in A/cm2)

We are considering the use of the solar cell for terrestrial applications. So, to account for the incident sunlight, AM1.5G illumination was considered in the simulation code, as this is the standard terrestrial illumination. According to this, the solar irradiance, E, is taken to be 1000 W/m2, or, 0.1 W/cm2. It was also considered that the device is working under 1 sun i.e. no concentrator is used.

Using Equation (9), the energy conversion efficiency was calculated.

1.2 Heterojunction Solar Cells

A heterojunction is a p-n junction formed between two different semiconducting materials. Heterojunctions have got numerous applications in optoelectronic devices [6]. Heterojunction solar cells generally employ a p-n or p-i-n structure. In the simplified p-n structure, one material essentially works as an absorber, while the other can be a window layer, or another absorber [7].

The absorber is the functioning layer for optical absorption and generation of electron-hole pairs. The window layer is usually a high bandgap material which is highly transparent to light, so that it can allow almost all the incident photons to reach the absorber.

Heterojunction devices have an inherent advantage over homojunction devices, which require materials that can be doped both p- and n-type. Many semiconducting materials can be doped either p-type or ntype, but not the both. Heterojunctions do not suffer from this limitation. So, many promising materials with good optical absorption capabilities can be investigated to produce optimal cells [8].

Again, a high-bandgap window layer reduces the cell's series resistance, and improves the output voltage [8]. It also helps to reduce recombination of minority carriers at the metal-semiconductor interface around the contacts [9].

For solar cells and other optoelectronic components, it is not sufficient to choose materials with suitable bandgap values and bring them to form a junction. It is also important to make sure that the chosen materials form a junction such that the interface is as much free of energy states in the forbidden band as possible, in order to prevent additional recombination of carriers and carrier trapping [9]. Material combinations satisfying such conditions are not very common. However, many combinations of III-V compounds, especially the ternary compounds based on GaAs, satisfy these criteria to large extents [9].

1.3 III-V Compounds as Photovoltaic Materials

III-V semiconductors typically have the Zincblende crystal structure (except for the Nitrides), with a lattice constant varying in the range of 5.4 to 6.2 Å, depending on the material [14]. Along with the binary compounds, there are also ternary and quaternary compounds available. Among all the III-V compounds, the most widely used one for solar cells and many other applications is GaAs, due to its optimum direct bandgap (1.42 eV). Besides this, GaAs has got high electron mobility (8500 cm2/ V-s), which makes it attractive for all types of solid-state devices. Single-junction solar cells fabricated from GaAs have achieved efficiency values as high as 28% [15]. Another promising III-V binary compound for the base layer of a solar cell is InP, which has an energy gap of 1.344 eV. Solar cells fabricated with monocrystalline InP have resulted in efficiencies around 22% [15]. Other compounds like AlxGa1-xAs, GaxIn1-xAs, GaxIn1-xP and AlxGa1-xAsyP1-y have been frequently used in multijunction solar cells [12, 16]. High bandgap materials like GaP (Eg=2.26 eV) and AlAs (Eg=2.16 eV) have been utilized as the window layer of heterojunction solar cells [13].

The III-V Nitrides typically have Wurtzite lattice structure (except for BN), and they can provide a very wide range of bandgap variation. Application of ternary III-V Nitrides, such as AlxGa1-xN, has been investigated for multijunction cells in recent years [17].

1.4 Drawback of III-V Solar Cells

The problem associated with III-V solar cells is that these cells are very expensive, compared to the commonly used terrestrial solar cell technologies [18]. This is mainly due to the high fabrication cost of III-V materials, along with the unavailability of necessary fabrication technology in few cases. So, the use of III-V solar cells is still limited to space applications, where the efficiency is prioritized over the cost [19, 20]. Utilization of such solar cells for terrestrial applications requires reduction of materials processing and fabrication costs. Another way to address this problem is to use concentrators with solar cells. Concentrated solar cells can give up to 2000 times the power output of a solar cell working under 1 sun, depending on the concentration level. Though concentrators are very expensive, they can offer a good trade-off between the PV system cost and the achievable high efficiency [21].

1.5 Research Outlines

In our work, we have introduced, characterized and optimized a novel III-V heterojunction solar cell using ADEPT/F simulator that incorporates an AlxGa1-xAs heterojunction. Here, the AlxGa1-xAs layer functions as the active (absorber) layer of the cell. A highly doped bottom layer of GaAs was also introduced in the design, which works as a Back Surface Field (BSF) layer. Ge substrate is used for the structure. Alloy composition of the ternary compounds was optimized for higher efficiency. The best design, which yields 21.4% efficiency, suffers from some basic difficulties in fabrication. In order to solve this, the issue of critical layer thickness with lattice mismatch was addressed carefully, and the revised design achieved 17.03% efficiency. A cost-effective thin film solar cell design was also proposed in the end.

1.6 Novelty in the Work

Till now, there is no evidence of heterojunction solar cells fabricated using AlxGa1-xAs /heterojunction. This work theoretically analyses the outcomes of applying this heterojunction in solar cells, along with the fabrication issues, discussed at the end of the work.

Chapter 2- The Design

2.1 Choice of Materials

2.1.1 Choice of Layer Materials

The top layer material, ZnS has an energy gap of 3.6 eV [28], a dielectric constant of 8.9 [28], and a lattice constant of 5.409 Å [27]. So far, this material has been extensively used to fabricate hetero-junction solar cells [20]. The reason behind choosing this material as the top layer is its high band gap. The top layer has been kept very thin (50 nm) and this layer plays a very minor role in optical absorption. Theoretically, it absorbs all the photons with energy greater than or equal to 3.6 eV, but it transmits all the photons having less energy than its band gap [29]. Now, photons with energy less than 3.6 eV correspond to wavelength greater than 0.34 μm [30], which constitute a good portion of the solar spectrum. Besides this, the thinness of the top layer does not allow it to absorb a large number of photons, so a considerable number of photons with energy greater than 3.6 eV are supposed to surpass the top layer for being absorbed in the next layers.

The middle layer (absorber) material, when we used elemental, Si, has an energy gap of 1.11 eV, and a lattice constant of 5.43 Å. This band gap is near the optimum band gap (1.4 eV) for a solar cell absorber. 1.11 eV corresponds to a wavelength of 1.12 μm. The highest wavelength present in visible light is around 0.78 μm, so it is evident that the middle layer absorbs the majority of photons transmitted from the top layer. To facilitate this absorption, the middle layer thickness is kept sufficiently high (1μm), with respect to the top layer thickness.

A p-type GaAs layer played the role of a Back Surface Field (BSF) layer. It was doped at $10^{18}\ cm^{-3}$. BSF layer is like a passivating layer for the rear surface of the cell. It has a much higher doping level than its adjacent layer, and their interface, as a result, acts like a barrier. An electric field is formed at the interface which prevents minority carrier flow from the base layer to the rear surface. So, the minority carrier concentration in the base is kept at higher levels [31].GaAs has a bandgap of 1.43 eV [28]. So, apart from providing passivation, this layer plays a less significant role in absorbing the photons with energy higher than 1.43 eV. As a total effect, after using this third layer, the output parameters are greatly improved.

2.1.2 Choice of Substrate

Germanium is a widely-used substrate for both heterojunction and multijunction solar cells. We needed to make a choice between Ge and GaAs as the substrate material. Germanium has almost the same lattice constant (5.658 Å) [28] as GaAs (5.65325 Å) [28]. The thermal expansion coefficients of these two materials are also similar. But the advantage that Germanium offers over GaAs as a substrate is its low cost and high mechanical strength. Due to this high mechanical strength, compared to GaAs, thinner Ge wafers can be fabricated [32].

2.1.3 Results and Discussion for the Design

The top layer was heavily n-doped at a doping concentration of $1\times10^{18}cm^{-3}$. The base layer doping concentration was kept at $1\times10^{16}cm^{-3}$. Substrate doping concentration was $1\times10^{16}cm^{-3}$. Bottom layer thickness is 100nm. Figure 2.1 below shows the light J-V characteristics graph obtained for this design.

Figure 2.1 shows that the initial design yields an open-circuit voltage (V_{oc}) of 0.8982 V, and the short-circuit current density (J_{sc}) is 0.0377 mA/cm^2 . Fill factor (FF) was calculated using the formula given in (6). Calculated fill factor is 0.8721.

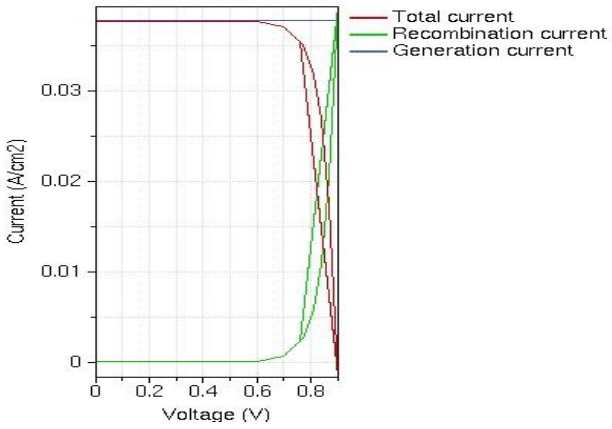

Fig. 2.1 Light J-V characteristics

The working conditions for the solar cell (solar irradiance, temperature, concentration level) were considered as mentioned in section 1.1.3. The efficiency is calculated using equation (9). For this design, the calculated efficiency, ŋ = 19.53%.

The next figure 2.2 shows the schematic diagram of the heterojunction solar cell we designed.

Fig. 2.2 Schematic diagram of the ZnS/Si heterojunction solar cell

Remarks

In this chapter, the light J-V characteristics curve of a design of the ZnS/Si heterojunction solar cell has been simulated under AM1.5G illumination with the effect of introducing a GaAs BSF layer on the energy conversion efficiency has been illustrated through the simulation results. Finally, under 1 sun, an energy conversion efficiency of 19.53% has been reported, for the device shown schematically in Figure 2.2.

Chapter 3- The Software Simulation

3.1 About The Software

3.1.1 Adept

ADEPT solves Poisson's equation coupled with the hole and electron continuity equations in one spatial dimension in compositionally nonuniform semiconductors. It was originally written to model solar cells fabricated from a wide variety of materials, including amorphous silicon, copper indium diselenide, and cadmium telluride. However, since material parameters (band gap, mobility, etc.) can be input by the user, devices fabricated from any material for which these parameters are known can be modeled. Dark I-V, light I-V, and spectral response of solar cells (or any two terminal devices) can be computed. Plots of many internal parameters, such as carrier density, recombination, electric field, etc., can be plotted at any operating point.

Homostructures and heterostructures, both abrupt and graded, can be modeled. Solar cell material systems modeled include ZnO/CdS/CIS, ZnO/CdS/CIGS, CdS/CdTe, a-Si, Si, AlGaAs/GaAs, GaSb, InP, and several others.

ADEPT/F simulator was written by Jeffrey L. Gray. User interface for launching simulations and analyzing results created by Michael McLennan.

3.2 Simulation Parameters

3.2.1 Band-gap (E_g)

In solid-state physics, a band gap, also called an energy gap or bandgap, is an energy range in a solid where no electron states can exist. In graphs of the electronic band structure of solids, the band gap generally refers to the energy difference (in electron volts) between the top of the valence band and the bottom of the conduction band in insulators and semiconductors [15]

In a semiconductor heterostructure, two different semiconductors are brought into physical contact. In practice, different semiconductors are “brought into contact” by epitaxially growing one semiconductor on top of another semiconductor. We classify heterostructures according to

the alignment of the bands of the two semiconductors. Three different alignments of the conduction and valence bands and of the forbidden gap shows the most common alignment which will be referred to as the straddled alignment or "Type I" alignment. GaAs / $Al_xGa_{1-x}As$ heterostructure, exhibits this straddled band alignment [10] . In staggered lineup the steps in the valence and conduction band go in the same direction. The staggered band alignment occurs for a wide composition range in the $Ga_xIn_{1-x}As$ / $GaAs_ySb_{1-y}$ material system [1 1] . The most extreme band alignment is the broken gap alignment. This alignment occurs in the InAs / GaSb material system [12]. Both the staggered lineup and the broken-gap alignment are called "Type II" energy band alignments.

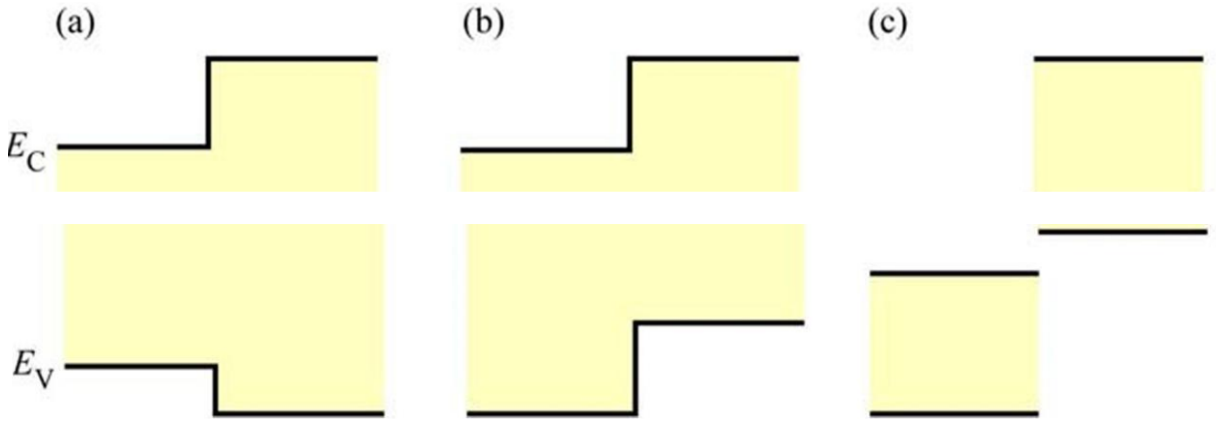

Fig.3.1: (a) the straddled alignment, (b) staggered lineup alignment (c) broken gap alignment

$Al_xGa_{1-x}As$, has an energy gap of 1.424 eV to 2.168 [13], a dielectric constant of 12.9 to 10.6 [13]. This material has been extensively used to fabricate hetero-junction and tandem solar cells [6]. Theoretically, the energy which is greater than or equal 1.424 eV to 2.168 is absorbed in this layer, but it transmits all the photons having less energy than its bandgap [5].

$x<0.45$ for $1.424+1.247x$ eV ---------- [13]

$x>0.45$ for $1.9+0.125x+0.143x2$ eV ---------- [13]

Gallium arsenide (GaAs) is a compound of the elements gallium and arsenic. It is a III-V direct bandgap semiconductor with a zinc blende crystal structure. It has a bandgap of 1.424ev and dielectric constant 12.9.

Germanium is a widely-used substrate for both hetero-junction and multi junction solar cells. We choice Ge as the substrate material. Germanium has almost the same lattice constant (5.658 Å)

[13] as GaAs (5.65325 Å) [13]. Germanium is chosen because of it's low cost and mechanical strength although it has same thermal expansion coefficient.

3.2.2 Dielectric Constant (Ks)

The dielectric constant is the ratio of the permittivity of a substance to the permittivity of free space. It is an expression of the extent to which a material concentrates electric flux, and is the electrical equivalent of relative magnetic permeability. [14]

As the dielectric constant increases, the electric flux density increases, if all other factors remain unchanged. This enables objects of a given size, such as sets of metal plates, to hold their electric charge for long periods of time, and/or to hold large quantities of charge. Materials with high dielectric constants are useful in the manufacture of high-value capacitors. [14]

The dielectric constant of GaAs and Ge is 12.9[7] and 16.2[8] respectively:

For $Al_xGa_{1-x}As$, this equation is used:

$$12.90-2.84x$$ ---------- [9]

3.2.3 Refractive Index (ndx)

In optics the refractive index or index of refraction n of an optical medium is a dimensionless number that describes how light, or any other radiation, propagates through that medium [16]. It is defined as,

$$n = \frac{c}{v}$$

where c is the speed of light in vacuum and v is the speed of light in the substance. For example, the refractive index of water is 1.33, meaning that light travels 1.33 times faster in a vacuum than it does in water.

Refractive index of GaAs and Ge is 3.00[7] and 4.00[8] respectively.

For $Al_xGa_{1-x}As$, the equation is:

$$n=3.3-0.53x+0.09x^2$$ ---------- [22]

3.2.4 Density of States (n_c & n_v)

In solid-state and condensed matter physics, the density of states (DOS) of a system describes the number of states per interval of energy at each energy level that are available to be occupied by electrons. Unlike isolated systems, like atoms or molecules in gas phase, the density distributions are not discrete like a spectral density but continuous. A high DOS at a specific energy level means that there are many states available for occupation. A DOS of zero means that no states can be occupied at that energy level. In general, a DOS is an average over the space and time domains occupied by the system. Local variations, most often due to distortions of the original system, are often called local density of states (LDOS). If the DOS of an undisturbed system is zero, the LDOS can locally be non-zero due to the presence of a local potential. [21]

There is two kinds of effective density of states conduction band effective density of states (n_c) and valence band effective of density (n_v). The conduction band effective density of states (n_c) and valence band effective of density (n_v) is fixed value for Ge and GaAs. For Ge $n_c=1x10^{-19}$ cm^{-3}[8] and $n_v=5x10^{-18}cm^{-3}$[8].For GaAs $n_c=4.7x10^{-17}$ cm^{-3}[7]and $n_v=9.0x10^{-18}cm^{-3}$[7].

For $Al_xGa_{1-x}As$, the equation is:

n_c: $x<0.41$ for $2.5\cdot10^{19}\cdot(0.063+0.083x)3/2$ cm^{-3} ---------- [8]
$x>0.45$ for $2.5\cdot10^{19}\cdot(0.85-0.14x)3/2$ cm^{-3}
n_v: $2.5\cdot10^{19}\cdot(0.51+0.25x)3/2$ cm^{-3} ---------- [8]

3.2.5 Electron Mobility (μ_n)

In solid-state physics, the electron mobility characterizes how quickly an electron can move through a metal or semiconductor, when pulled by an electric field [27]. The term carrier mobility refers in general to both electron and hole mobility in semiconductors.

When an electric field E is applied across a piece of material, the electrons respond by moving with an average velocity called the drift velocity,vd. Then the electron mobility μ is defined as

$$Vd = \mu E$$

Electron mobility is almost always specified in units of $cm^2/(V\cdot s)$.

Electron mobility for GaAs and Ge is <=8500 $cm^2v^{-1}s^{-1}$ and <=3500 $cm^2v^{-1}s^{-1}$.

For $Al_xGa_{1-x}As$, the electron mobility is calculated by,

$0<x<0.45$ for $8\cdot10^3-2.2\cdot10^4x+10^4\cdot x^2$ cm^2 V^{-1} s^{-1} ---------- [29]
$0.45<x<1$ for $-255+1160x-720x^2$ cm^2 V^{-1} s^{-1} ----------[29]

3.2.6 Hole Mobility (μ_p)

Hole Mobility is the parameter which is a measure of hole scattering in a semiconductor; proportionality factor between hole drift velocity and electric field as well as conductivity and hole concentration in semiconductor; due to its higher effective mass, hole mobility is typically significantly lower than electron mobility [30].

Hole mobility for GaAs and Ge is <=1900 $cm^2v^{-1}s^{-1}$ and <=400 $cm^2v^{-1}s^{-1}$. For
For $Al_xGa_{1-x}As$, the hole mobility can be calculated by,

$370-970x+740x^2\ cm^2\ V^{-1}\ s^{-1}$ ---------- [29]

Remarks:

In this chapter, it is discussed about the different parameters that are for the simulation and their values for different mole fraction.

Chapter 4 - Optimization

4.1 Insight

The electrical properties of III-V ternary alloys such as bandgap, carrier mobility, dielectric constant [28] etc. can be greatly varied by changing the alloy composition. This change also affects various optical properties like absorption coefficient [28], refractive index [27] etc. In this chapter, simulation results have been analyzed for varying alloy compositions of the ternary alloy- AlxGa1-xAs which constitute the base of the solar cell. The base layer material, AlxGa1-xAs, can have a varying energy gap of 1.55-2.13 eV, as the Aluminum mole fraction x varies from 0.1 to 0.9. It becomes a direct bandgap material from an indirect one as x becomes lower, the transition point located at x= 0.45 [28]. Besides bandgap, change in alloy composition alters many other electrical and optical properties of an alloy, as previously mentioned. Hence, an analysis of efficiency variation of the device with changing alloy composition at the layers can give an insight on how the alloy composition should be fixed at each layer for the maximization of energy conversion efficiency.

4.2 Methodology

Before conducting simulations, some default values for thickness, doping concentration and alloy composition for each layer were fixed. Table 4.1 summarizes these default values.

Table 4.1

Default Values of Device Parameters for Each Layer

Device parameters	**Top layer (Emitter) (ZnS)**	**Middle Layer (Base) $Al_xGa_{1-x}As$**	**Bottom Layer (BSF Layer) GaAs**	**Substrate (Ge)**
Layer thickness (μm)	0.5	1	0.1	100
Doping Type	n	P	p	p
Doping Conc. (cm^{-3})	1×10^{18}	1×10^{16}	1×10^{18}	1×10^{16}
Value of x for the Alloy	-	0.1	-	-

Afterwards, simulations were done by varying the value of x for the base layer alloy (AlxGa1-xAs) from 0.1 to 0.6, in steps of 0.1. Efficiency versus x (Aluminum mole fraction) curve was obtained in the similar manner discussed above. Further simulations (for x=0.7 to 0.9) were not conducted, as the nature of efficiency variation against varying alloy composition was already evident from the graph.

4.3 Results and Discussions

4.3.1 Varying Alloy Composition in $Al_xGa_{1-x}As$ (Middle Layer)

Aluminum mole fraction (x) in AlxGa1-xAs was varied from 0.1 to 0.6, in steps of 0.1. The light J-V characteristics curves for x = 0.3- 0.6 are given in figures 4.11- 4.14. The simulation results are summarized in table 4.3. A plot of efficiency versus Aluminum mole fraction (x) in AlxGa1-xAs is given in figure 4.15. It is to be mentioned that simulations for x > 0.6 in AlxGa1-xAs were not conducted, because Al0.7Ga0.3As has an indirect bandgap of 1.85 eV [38], which is far from the optimum bandgap (1.4 eV) for the absorber of a solar cell [11]. The bandgap becomes even higher for higher values of x.

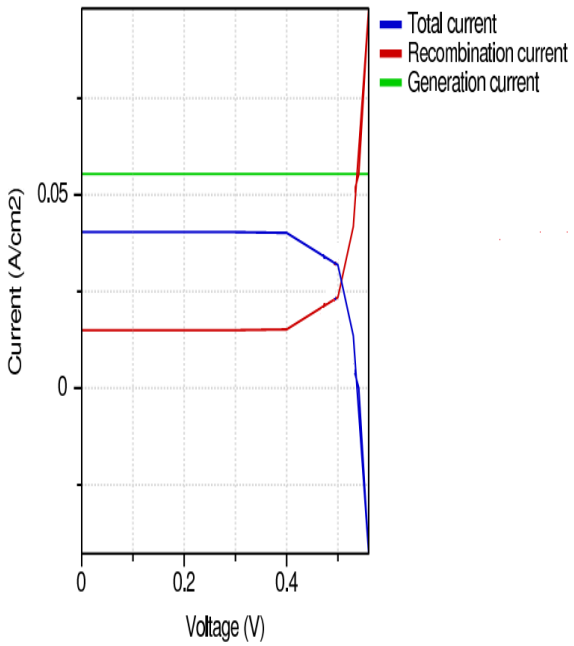

Fig. 4.1 Light J-V characteristics curve with x= 0.3 in $Al_xGa_{1-x}As$.

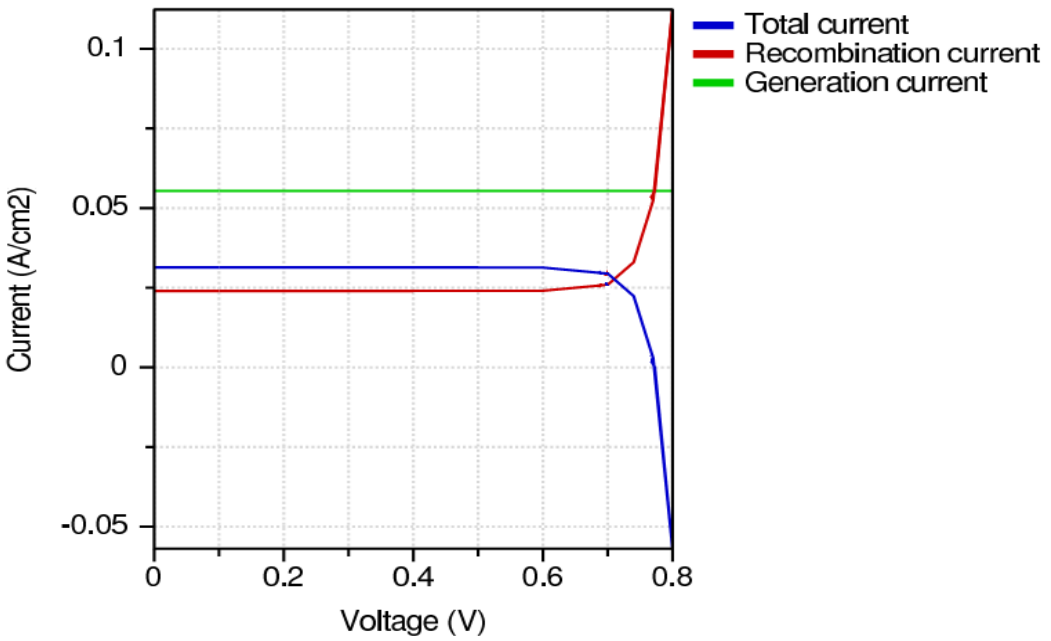

Fig. 4.2 Light J-V characteristics curve with x= 0.4 in $Al_xGa_{1-x}As$.

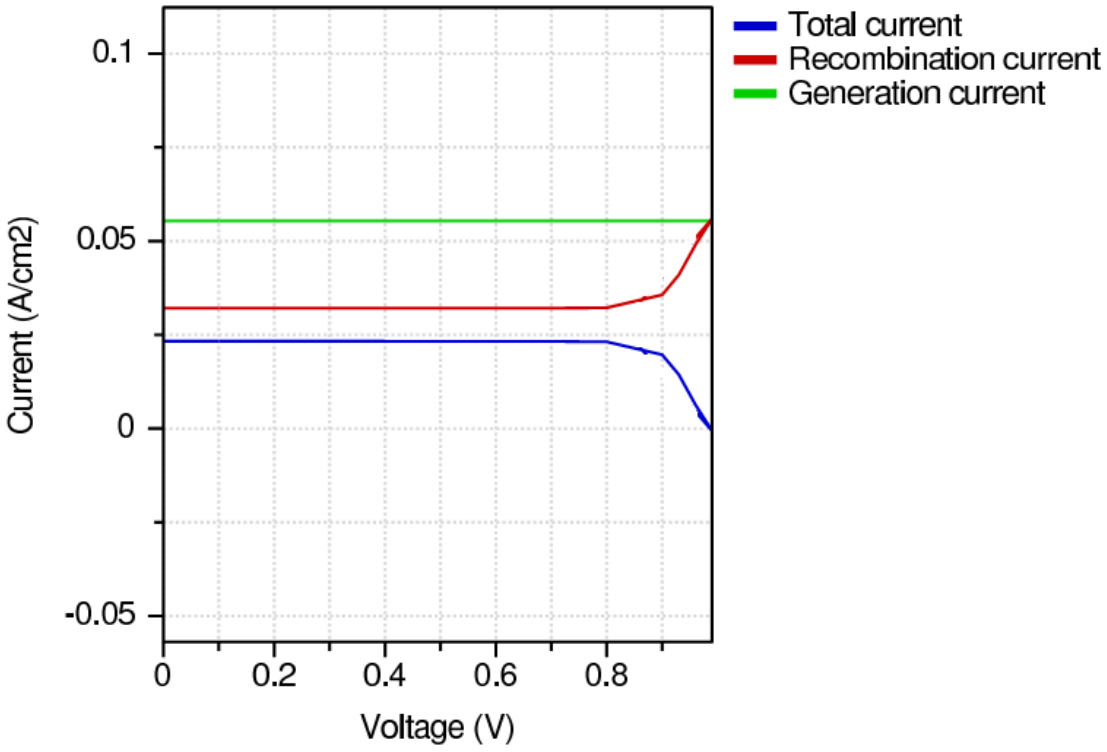

Fig. 4.3 Light J-V characteristics curve with x= 0.5 in $Al_xGa_{1-x}As$.

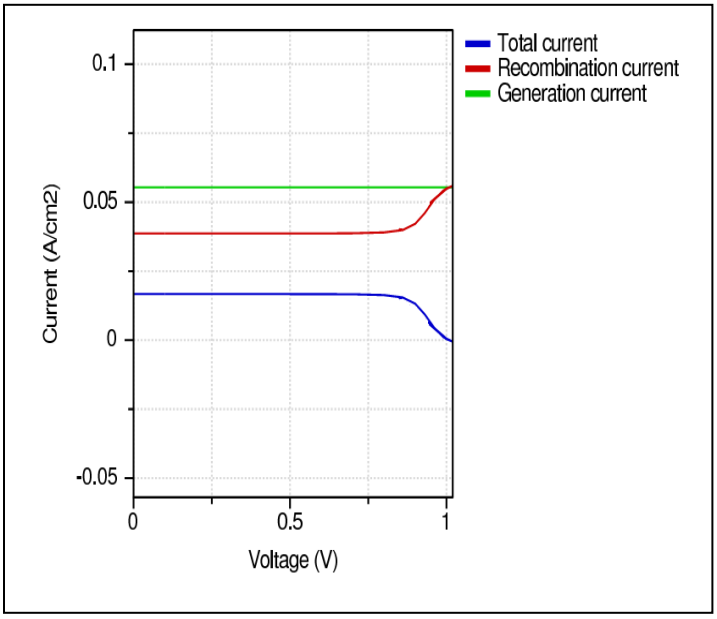

Fig. 4.4 Light J-V characteristics curve with x=0.6 in $Al_xGa_{1-x}As$.

Table 4.2

Simulation Results for Different Alloy Compositions of Aluminium Gallium Arsenide

x in $Al_xGa_{1-x}As$	**Energy Gap (eV)**	**Jsc (mA/ cm^2)**	**Voc (V)**	**FF**	**n (%)**
0.1	0.5	55.92	0.075	0.4136	1.73
0.2	0.75	47.14	0.3087	0.7264	10.57
0.3	1.0	40.4	0.5408	0.814	17.78
0.4	1.23	31.4	0.7726	0.8568	20.79
0.5	1.48	23.29	0.9867	0.8809	20.24
0.6	1.75	16.71	1.0043	0.8825	14.81

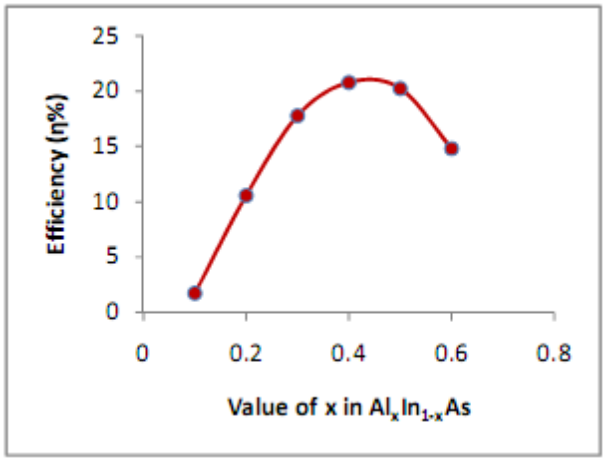

Fig. 4.5 Graph of efficiency versus Aluminium mole fraction in $Al_xGa_{1-x}As$.

The graph in figure 4.5 shows that the highest level of efficiency is obtained when Aluminium mole fraction in AlxGa1-xAs is between 0.4 and 0.5. So, the value of x in AlxGa1-xAs should be kept 0.4 ~ 0.5 for optimization.

4.3.2 Optimization of Alloy Composition

4.3.2.1 First Design

In this design, Aluminium mole fraction in AlxGa1-xAs is taken as 0.5 (x= 0.5). Every other device parameter is kept the same as the first design. The light J-V characteristics graph obtained for this design is shown in figure 4.27.

From figure 4.6, values of the open-circuit voltage (Voc) and the short-circuit current density (Jsc) are found as 1.0179 V and 23.72 mA/cm^2, respectively. Clearly, the voltage has increased, but at the cost of a reduction in current. The calculated fill factor is 0.8837, and the resulting efficiency is 21.34%. So, the efficiency has increased as the Al mole fraction in AlxGa1-xAs is taken as 0.5.

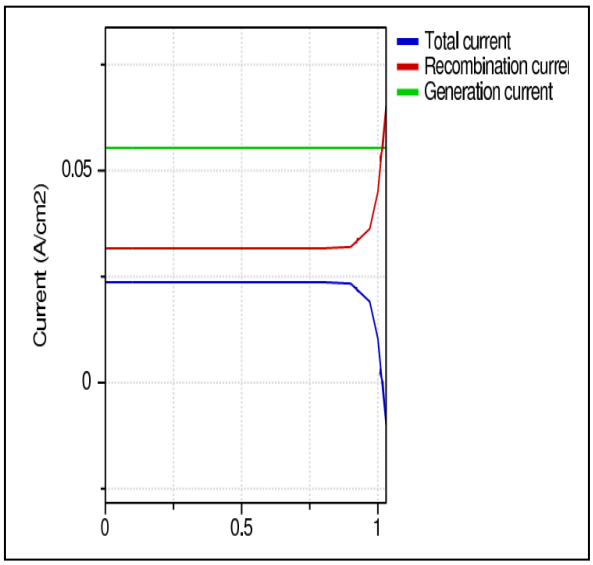

Fig. 4.6 Light J-V characteristics of the first design.

4.3.2.2 Second Design

In this design, Aluminium mole fraction in AlxGa1-xAs is taken as the default value (x= 0.48) listed in table 4.1. Every other device parameter is kept the same as the first design. Figure 4.28 shows the light J-V characteristics graph obtained for this design.

For the second design, the obtained open-circuit voltage is 0.9607 V, while the short-circuit current density is 25.34 mA/cm^2. The calculated fill factor is 0.8785. Finally, the calculated efficiency is 21.39%. This is the highest efficiency achieved from the two proposed designs.

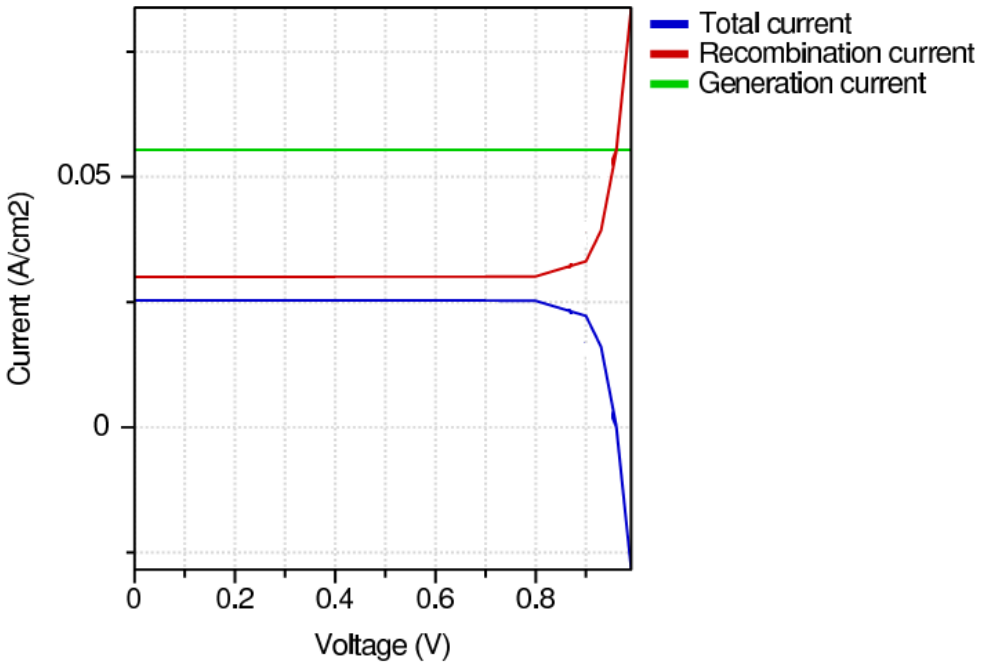

Fig. 4.7 Light J-V characteristics of the second design.

4.3.3 Approach for Maximizing the Efficiency

From the analysis of the efficiency variation curves and the outcomes of the proposed designs, it is obvious that in order to achieve the maximum possible efficiency from the ZnS /AlxGa1-xAs heterojunction solar cell, Aluminium mole fraction in AlxGa1-xAs should be kept somewhere between 0.4 and 0.5. Inspecting the efficiency versus Aluminium mole fraction curve for AlxGa1-xAs more precisely suggests that the Aluminium mole fraction should be kept between 0.45 and 0.5.

Remarks

In this chapter, dependence of energy conversion efficiency on alloy composition has been investigated in details for the ZnS / AlxGa1-xAs heterojunction solar cell. Effect of change in alloy composition on efficiency has been analysed separately for each layer of the device. This analysis will be helpful in selecting materials with optimum combination of bandgaps for fabricating heterojunction solar cells. The results found in this chapter can provide a better insight into the way of alloy composition optimization in heterojunction and multijunction solar cells fabricated from ternary and quaternary alloys for achieving the highest possible efficiency.

Chapter 5- Practical Solutions for Fabrication Purpose

5.1 Problems in the Proposed Designs

5.1.1 Lattice Mismatch

In the final best design proposed, ZnS, $Al_{0.48}Ga_{0.52}As$ and GaAs were taken as the top, middle and bottom layer materials, respectively. Substrate for the structure was Germanium (Ge). The major problem in this design is the high lattice mismatch between the layers. Germanium has a lattice constant of 5.65 Å [14]. Now, the growth of the BSF layer (GaAs) on the substrate demands perfect lattice-matching between these two materials, so that the structure is defect-free [14]. But the lattice constant of GaAs is 5.6938 Å [28], which results in a lattice mismatch of 0.77% with Ge. Though the mismatch is small, it restricts the growth of GaAs on Ge to a critical layer thickness of around 12 nm [40].

$Al_{0.48}Ga_{0.52}As$ has a lattice constant of 5.8686 Å . So, the lattice mismatch between GaAs and $Al_{0.48}Ga_{0.52}As$ is 2.98%, which is pretty high, and gives a critical layer thickness of 2 nm only [40].

ZnS has a lattice constant of 5.66032 Å [28], and the lattice mismatch between ZnS and $Al_{0.48}Ga_{0.52}As$ is 3.55%. This gives a critical layer thickness of around 2 nm for epitaxial growth [40].

This issue is of lattice mismatch is vital, as it determines whether the device can be fabricated to give optimum device performance or not. High defect density degrades the quality of the structure, and results in poor performance and device lifetime. The possible solutions to this problem have been discussed in later sections, with appropriate references.

5.1.2 High Fabrication Cost

The designs proposed in sections 4.3.2.1 and 4.3.2.2 yield nearly the maximum possible efficiency for this particular heterojunction solar cell, but the issue of materials and fabrication cost was not considered while proposing the designs. The only target there was to maximize the efficiency. But the fabrication cost of ternary III-V compounds is high [41], and bulk III-V solar cell is not a cost-effective option. So, the reduction of layer thickness is necessary for the

proposed designs, especially for the absorber layer ($Al_{0.48}Ga_{0.52}As$), as it was kept very thick. A thicker absorber will surely absorb a greater number of photons, but there must be a trade-off between the desired efficiency and the material cost.

5.2 Practical, Cost-effective Designs

5.2.1 Solving the Lattice Mismatch Issue

One way to solve the lattice mismatch problem between two adjacent layers is to apply a buffer layer in between. The lattice constant of the buffer layer is intermediate to that of the two adjacent layers, and it helps to adjust the lattice mismatch to some extents. Now, it is easy to find a buffer layer for adjusting the lattice mismatch between the bottom layer and the substrate, as the mismatch is small. But the major problem is to find a material as the buffer layer in between the $Al_{0.48}Ga_{0.52}As$ and GaAs layers, because the $Al_{0.48}Ga_{0.52}As$ absorber must be sufficiently thick, and the defect-free growth of a thick $Al_{0.48}Ga_{0.52}As$ layer on a material requires perfect lattice-matching between them. The ideal lattice constant of a buffer layer that can be applied between $Al_{0.48}Ga_{0.52}As$ and GaAs is around 5.78 Å, which still generates 1.5% lattice mismatch with the $Al_{0.48}Ga_{0.52}As$ layer, and gives a critical thickness of around 7 nm only [40]. So, using a buffer layer between $Al_{0.48}Ga_{0.52}As$ and GaAs cannot be a solution.

We note from section 3.2.3 that an ultra-thin emitter layer improves the performance of the solar cell, as it acts as a window layer for the cell. This is why we used a 50 nm ZnS layer in our final optimized design in section 4.3.4. The results in section 3.2.3 indicate that window layers thinner than 50 nm will give even better performance. So, we do not actually need any buffer layer between ZnS and $Al_{0.48}Ga_{0.52}As$, rather we can go for an ultra-thin window layer which has a thickness equal to the critical layer thickness in this case (2 nm).

Growth of a 2 nm layer can be done by e-beam evaporation (e-beam evaporators today can offer a deposition rate of 0.5 nm/ min or even less [42]), or some other deposition method that can provide low deposition rate.

Now, we are back to the problem of lattice mismatch between $Al_{0.48}Ga_{0.52}As$ and GaAs. As we have already discussed that the growth of a buffer layer is not a feasible idea, we move on to a new approach. We note that the lattice constant of GaAs can be changed if we change the alloy composition of the material, and GaAs is perfectly lattice matched to $Al_{0.48}Ga_{0.52}As$ [27, 28]. Now, section 4.3.3 suggests that reducing the Gallium mole fraction in GaAs degrades the efficiency of the solar cell; yet we have to follow this approach to ensure perfect lattice matching between the absorber and the BSF layer, so that the absorber can be grown in any desired thickness. So, we will be using GaAs as the BSF layer material in our practical designs, which will be proposed in section 5.2.2. We note that GaAs has a direct bandgap of 0.7734 eV, which is less than that of GaAs (1.28 eV). This will reduce the open-circuit voltage of the device, which will reduce the efficiency, as discussed in section 4.3.3.

A new problem arises that the lattice mismatch between $Ga_{0.47}In_{0.53}As$ and Ge is higher (3.7%) than it was for $Ga_{0.9}In_{0.1}As$. This gives a critical layer thickness for the growth of $Ga_{0.47}In_{0.53}As$ on Ge of slightly less than 2 nm [40]. This means that we should not allow the growth of > 2 nm thick $Ga_{0.47}In_{0.53}As$ epitaxial layer on Ge substrate. We observed in section 3.2.1 that the change of efficiency with changing BSF layer thickness is insignificant. However, we did not investigate this effect for thickness < 200 nm. Ultra-thin BSF layers may have significant impact on efficiency.

5.2.2 Cost Effective Solar Cell- a Thin Film Approach

As we mentioned in section 5.1.2, a trade-off is needed to be made between cell efficiency and material cost. We have already decided to use 2 nm thick emitter layer and BSF layer in the solar cell, for eliminating the effect of lattice mismatch. So, we bring back the highest efficiency design discussed in section 4.3.4.3, with three modifications- using $Ga_{0.47}In_{0.53}As$, instead of $Ga_{0.9}In_{0.1}As$ for the BSF layer; changing the top layer thickness to 2 nm, and changing the BSF layer thickness to 2 nm. Figure 5.1 shows the J-V characteristics curve for this design.

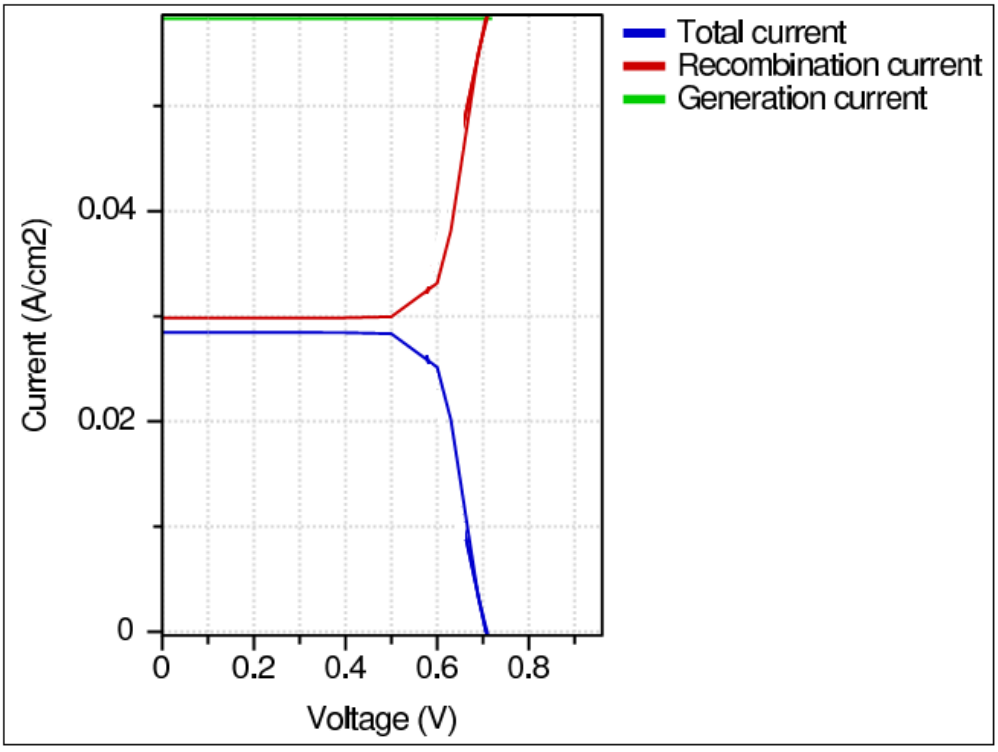

Fig. 5.1 Light J-V characteristics curve for the design of section 4.3.2.2 after modification.

The short-circiut current density for this design is 28.47 mA/ cm^2, open-circuit voltage is 0.7063 V, and the fill factor (FF), calculated using equation (6) is 0.8469. The calculated efficiency is 17.03%. We can see that the efficiency has decreased significantly, compared to the 21.39% efficiency in section 4.3.4.3, due to the reasons already discussed.

Now, we have conducted a number of simulations with varying base layer thickness values, in order to give us a good number of options for the efficiency and cost trade-off. Table 5.1 lists the simulation outcomes. A graph of efficiency versus middle layer thickness of the modified design is shown in figure 5.2.

The results shown in table 5.1 give few good design options that are cost-effective and moderately efficient. It is to be noted that thickness of the emitter and base (2 nm each) are negligible, when the base thickness is in the range of microns. So, we can consider the base thickness as the thickness of the cell (excluding the substrate thickness).

Table 5.1

Simulation Results for Varying Base Thickness of the Modified Design

Base Thickness (pm)	**Voc (V)**	**J_{sc} (mA/cm^2)**	**FF**	**Efficiency (n%)**
100	0.7063	28.47	0.8469	17.03
20	0.6419	28.33	0.8357	15.2
10	0.6208	28.13	0.8317	14.52
5	0.6004	27.66	0.8275	13.74
2	0.5706	25.95	0.821	12.16

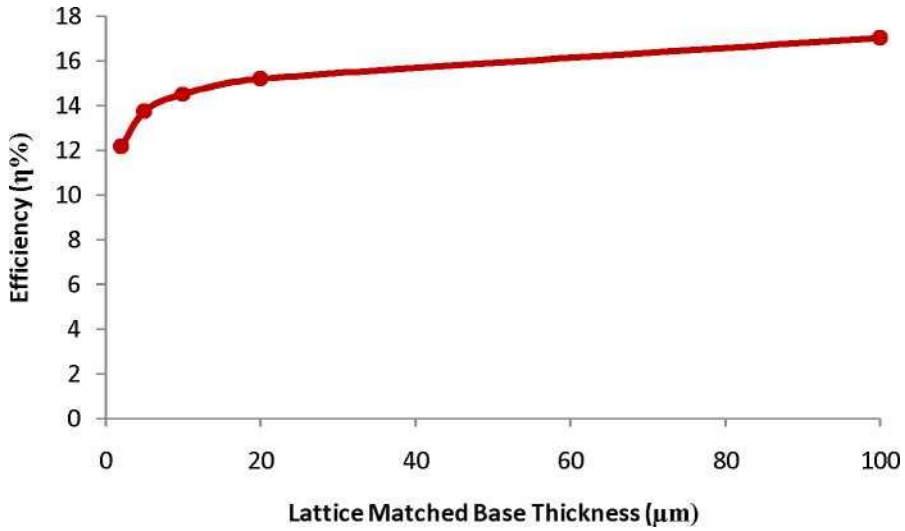

Fig. 5.2 Efficiency vs absorber thickness of the modified design.

We see from table 5.1, that a 10 µm thick cell yields an efficiency of 14.52%. The 5 µm cell can be an option for a thin film solar cell, which yields an efficiency of 13.74%. As a better thin film approach, we can consider the 2 µm cell (starting point of the graph), which gives an efficiency of 12.16%. The light J-V characteristics curve for the 2 µm cell is given in figure 5.3.

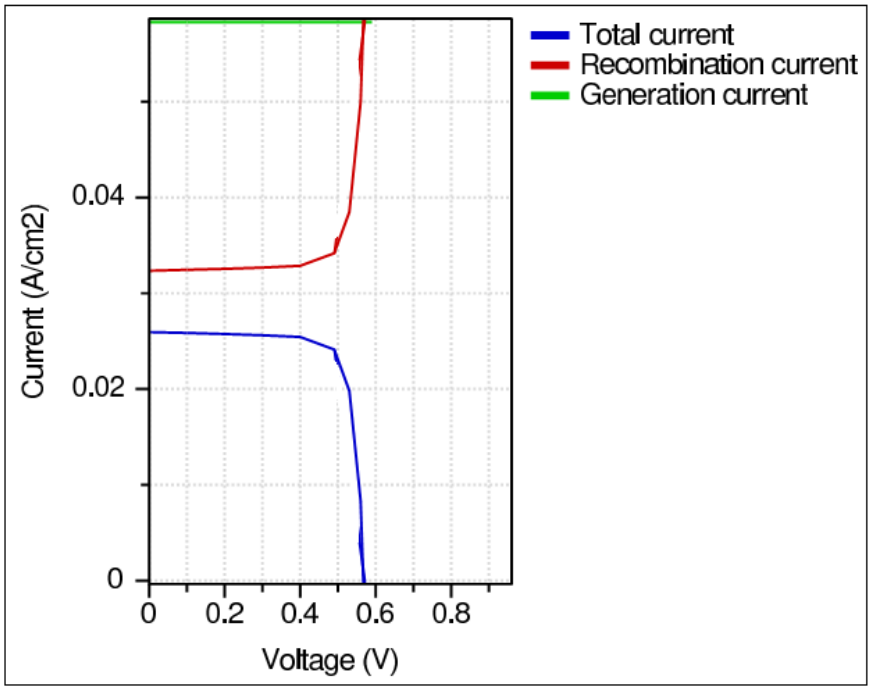

Fig. 5.3 Light J-V characteristics curve for 2 µm cell thickness (excluding substrate thickness).

5.2.3 About Substrate Doping

We can fabricate the device on Germanium wafer; the wafer being heavily p-doped (1×10^{18}cm ^{3}). One way to do this is to dope during crystal growth from the ingot. Heavily doped wafers are supposed to improve the solar cell performance to some extents [45].

5.2.4 About p-type Doping in $Al_{0.48}Ga_{0.52}As$

$Al_{0.48}Ga_{0.52}As$ is a less-investigated material for application in optoelectronic devices. So, we need to discuss about the realization of p-type doping in $Al_{0.48}Ga_{0.52}As$. $Al_{0.48}Ga_{0.52}As$ has an intrinsic carrier concentration of 1.6×10^{7} cm^{-3} (at 300 K) [46]. The electron affinity of $Al_{0.48}Ga_{0.52}As$ is 4.03 eV [47], which is moderate, and the material can be easily p-doped. Actually, both p-doping and n-doping are possible for $Al_{0.48}Ga_{0.52}As$, which is supported by previous works [25, 26, 48]. $Al_{0.48}Ga_{0.52}As$ p-n homojunction has been implemented very recently in thin film solar cells [25, 26].

5.3 A Better Approach

In the proposed cost-effective designs in section 5.2.2, we noticed that the efficiency has decreased, compared to the design in section 4.3.4.3, after using a $Ga_{0.47}In_{0.53}As$ BSF layer (which is lattice-matched to $Al_{0.48}Ga_{0.52}As$). This is mainly due to the low bandgap of $Ga_{0.47}In_{0.53}As$ (0.7734 eV), compared to that of $Ga_{0.9}In_{0.1}As$ (1.28 eV); this low bandgap degrades the open-circuit voltage of the solar cell drastically, as seen from table 5.1. The point is, if we use a $Ga_xIn_{1-x}As$ BSF layer, the x value must be kept at 0.47, for the growth of an $Al_{0.48}Ga_{0.52}As$ absorber on $Ga_xIn_{1-x}As$. The absorber must have a moderate thickness (which was 2 μm in our thin film design). So, the necessity of perfect lattice matching between the two materials ($Al_{0.48}Ga_{0.52}As$ and $Ga_xIn_{1-x}As$) cannot be compromised. So, in order to improve the output characteristics, we suggest the use of an InP substrate, instead of Ge. It is to be noted that InP is perfectly lattice-matched to $Al_{0.48}Ga_{0.52}As$ and $Ga_{0.47}In_{0.53}As$. Though InP is costlier than Ge [49], using InP for our solar cell is advantageous for two reasons- InP has a much higher bandgap (1.344 eV) than Ge, which improves the open-circuit voltage slightly; and the BSF layer can now be grown at any desired thickness. An ultra-thin BSF layer slightly degrades the efficiency of the cell, as previously mentioned.

Considering the issue of cost-effectiveness, we suggest our very final design of a thin film solar cell, where the $Al_{0.48}Ga_{0.52}As$ absorber is 2 μm thick, and the $Ga_{0.47}In_{0.53}As$ BSF layer has a thickness of 1 μm. The solar cell will be grown on InP substrate, instead of Ge. Every other design parameter is kept the same as the 2 μm solar cell, discussed in section 5.2.2. Simulation was conducted for this cell, and the light J-V characteristics curve is given in figure 5.4.

We note that this new thin film solar cell has a total thickness of 3 μm (excluding the substrate

thickness). The short-circuit current density (Jsc) was obtained as 26.03 mA/cm^2, the open-circuit voltage being 0.637 V, and the fill factor (FF) being 0.8348. The efficiency is calculated as 13.84%. We see, with this design, the open-circuit voltage is considerably improved, and so the efficiency.

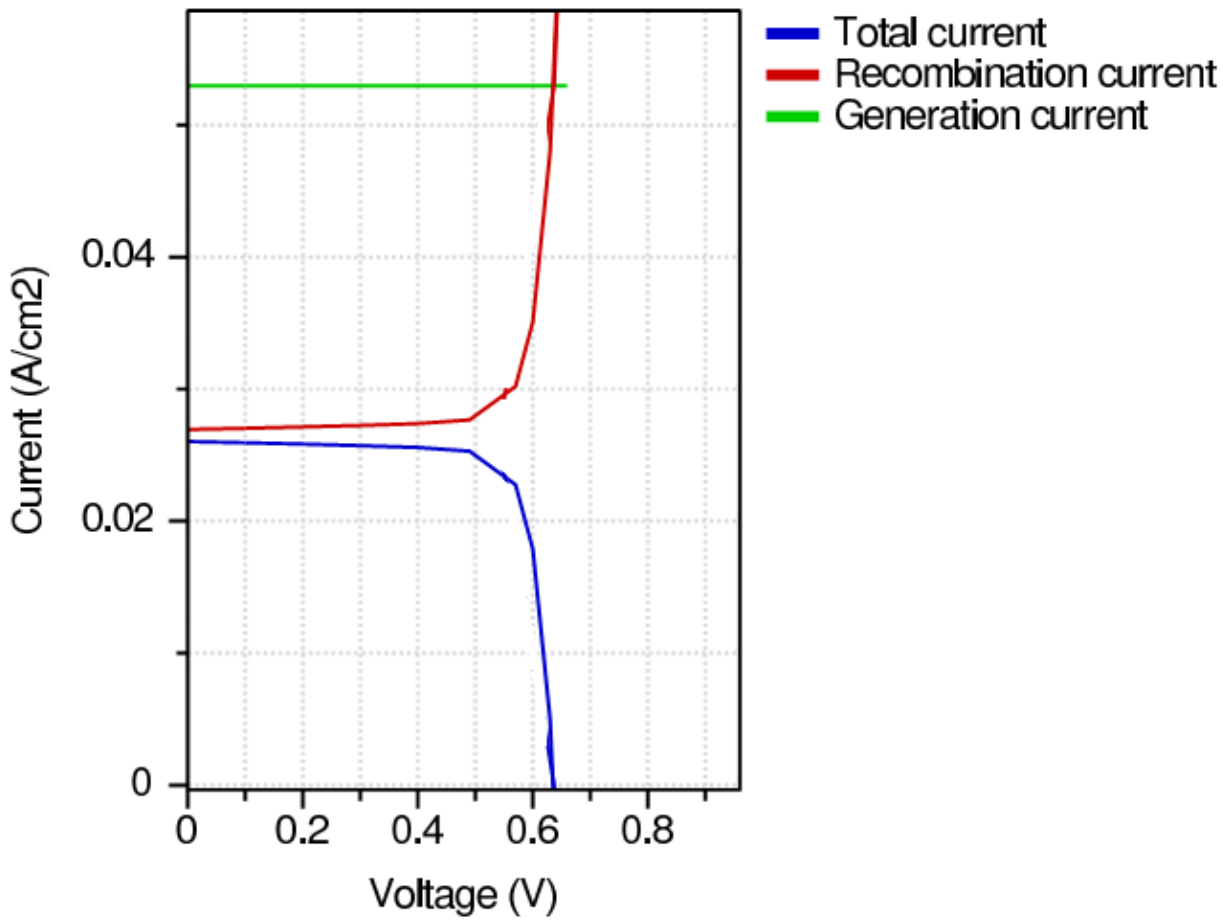

Fig. 5.4 Light J-V characteristics curve for the 3 μm cell on InP substrate.

Remarks

This chapter discusses in details the critical fabrication issues of our proposed solar cell, and proposes more practical and cost-effective designs. One significant contribution made in this chapter is the design of a thin film solar cell with our initial cell structure and materials. Finally, the substrate was changed to InP from Ge, which gave more improved results.

Chapter 6- Summary

6.1 Overview of the Work

In chapter 1, we have discussed the basic operational principles of solar cells, along with the basics of heterojunction solar cells. We have also discussed the application of III-V compounds in solar cells, with an investigation into the high-cost issue of III-V solar cells, which is the limiting factor for the mass fabrication of these solar cells. We have also given a brief outline of our research, and discussed the novelty in our device with appropriate references.

In chapter 2, we have introduced an initial design of an ZnS/$Al_{0.48}Ga_{0.52}As$ heterojunction solar cell, with its corresponding light J-V characteristics curve. Later, we have added a GaAs Back Surface Field (BSF) layer in the solar cell, which greatly improved the output characteristics of the solar cell.

In chapter 3, we discussed about the software we used in the simulation and different parameters that are used in simulation. In chapter the different values of these parameters for different mole fraction are also given.

In chapter 4, we have investigated the change in output characteristics of the device with varying alloy composition of the layer materials. Analysis was done separately for each layer material, to understand the effects more appropriately. The outcomes have been discussed, and the way of optimization of alloy composition at different layers was illustrated. Finally, we have proposed three high efficiency designs at the end of the chapter.

Up to chapter 4, the only target was to optimize the design parameters and material properties for achieving maximum efficiency. The proposed designs achieved pretty high efficiency values, but they were not investigated from the point of view of fabrication and cost-effectiveness.

Chapter 5 discusses these issues in details with practical solutions. This chapter discusses the critical issues of fabrication, and brings necessary modifications in the designs of chapter 4. Trade-off between cost and efficiency was done, and moderate efficiency values were reported for practical, low-cost designs. A thin film approach was taken in the end, and the resulting output characteristics curves have been discussed.

6.2 Major Contributions of the Work

The most important contribution of this research work is the **introduction of an ZnS / $Al_xGa_{1-x}As$ heterojunction as the working p-n junction of a solar cell**. $Al_xGa_{1-x}As$ is a less investigated material as the constituent of a solar cell, and **it has only been tried in**

homojunction solar cells very recently [25, 26]. **The advantage of forming a heterojunction of $Al_{0.48}Ga_{0.52}As$ with a high bandgap material is that, while $Al_{0.48}Ga_{0.52}As$ functions as the absorber of the cell ($Al_{0.48}Ga_{0.52}As$ has a direct bandgap of 1. 47 eV, which is near the optimum bandgap of 1.4 eV for the absorber of a solar cell [11]), the high bandgap upper layer can act as a window layer for the cell. This eliminates the necessity of a separate window layer.** Now, what opposes the realization of $Al_{0.48}Ga_{0.52}As$ in a useful heterojunction is the unavailability of a high bandgap material with a Zincblende structure, and the same lattice constant as $Al_{0.48}Ga_{0.52}As$. ZnS has a lattice mismatch of 3.55% with $Al_{0.48}Ga_{0.52}As$. Lattice mismatch limits the growth of the upper ZnS window layer on $Al_{0.48}Ga_{0.52}As$ to a very small critical thickness (≈ 2 nm) [40]. Now, **we have shown in our work (in section 3.2.3) that the efficiency is improved with an ultra-thin (few nanometers thick) window layer. We have also given the evidence of realization of very low deposition rates (0.5 nm / min or less) [42], which makes it possible to grow epitaxial layers which are only 2- 10 nm thick. So, it is possible to grow an ultra-thin (≈ 2 nm) window layer of ZnS on $Al_{0.48}Ga_{0.52}As$. This implies that an ZnS/ $Al_{0.48}Ga_{0.52}As$ heterojunction is implementable, and it gives improved performance for our particular device, as the bandgap of the window material (ZnS) is high (2.13 eV).**

Another contribution of the work is the **investigation into the output characteristics of the solar cell with Ga0.47In0.53As (lattice matched to Al0.48In0.52As) being applied as a back surface field (BSF) layer**. Another outcome of the work is the **evidence of superiority of InP over Ge as a substrate for this particular solar cell.**

The works done in chapter 3 and 4 provide **useful insights into the optimization of design parameters and material properties for maximizing the efficiency level** in III-V solar cells.

6.3 Future Work

It is already mentioned that while using an $Al_{0.48}Ga_{0.52}As$ absorber, it is advantageous to use a heterojunction instead of a homojunction, because this gives the option to use a high bandgap window layer as part of the p-n junction. In our final design, $Al_{0.9}Ga_{0.1}As$ was used as the window layer, which has an indirect bandgap of 2.13 eV. This is a pretty good choice, provided that we choose our window layer material from the III-V compounds. But actually, a window layer with bandgap higher than 2.5 eV will significantly improve the efficiency. Unfortunately, if we restrict our choice to those III-V compounds which have a maximum of 4% lattice mismatch (critical layer thickness of ≈ 1.2 nm) with $Al_{0.48}Ga_{0.52}As$, we do not have many options that give a high bandgap. It is to be noted that GaP and $Ga_xIn_{1-x}P$ with $x \approx 0.9$, have bandgap between 2.2-2.26 eV [28], but they have a lattice mismatch of around 7%, with $Al_{0.48}Ga_{0.52}As$. For < 4% lattice mismatch, we can choose AlAs (3.55% lattice mismatch) from the binary compounds, or $AlAs_{0.9}Sb_{0.1}$ (2.8% lattice mismatch) or $AlP_{0.65}Sb_{0.35}$ (2.9% lattice mismatch) from the ternary compounds, or $Al_{0.75}Ga_{0.25}P_{0.7}Sb_{0.3}$ (3.7% lattice mismatch) from the quaternary compounds, which provide bandgaps of 2.16, 2.08, 2.1 and 2.1 eV, respectively [14, 50]. Looking at these bandgap values, we can conclude that we do not have much better options than $Al_{0.9}Ga_{0.1}As$ from the III-V compounds to use as a window layer.

If the window layer is chosen from II-VI compounds, which have a Zincblende lattice, then we may have better options, like ZnSe (3.37% lattice mismatch with $Al_{0.48}Ga_{0.52}As$, bandgap of 2.7 eV) or ZnTe (3.81% lattice mismatch with $Al_{0.48}Ga_{0.52}As$, bandgap of 2.25 eV). These materials can be worked out in future to replace $Al_{0.9}Ga_{0.1}As$ in our proposed heterojunction solar cell for higher efficiency.

Another development that can be done in our solar cell is to eliminate the GaAs BSF layer from the final design of section 5.3. Since the InP substrate is heavily (≈ 1018 cm-3) doped, it can work as a BSF layer in absence of the GaAs layer (the reader is requested to refer to section 2.1.1 for the functional principle of the BSF layer). This will not change the results of section 5.3 significantly. As the substrate is very heavily doped with respect to the $Al_{0.48}Ga_{0.52}As$ absorber, it can effectively function as a BSF layer. So, we can have a thin film solar cell which is only 2 μm thick (excluding substrate thickness), and yet yield an efficiency of nearly 14%.

The solar cell introduced in this work does not have an anti-reflective (AR) coating to reduce photon loss due to reflection, or a bragg reflector that would increase the quantum efficiency of the cell. Including such layers in the solar cell would give higher efficiency.

Bibliography

1. Peter Gevorkian, *Sustainable energy systems engineering: the complete green building design resource*, p. 498,
McGraw-Hill Professional, New York, USA, 2007, ISBN: 978-0071473590.

2. Marius Grundmann, *The Physics of Semiconductors: An Introduction Including Nanophysics and Applications,*
2nd ed., p. 3, Springer-Verlag, Berlin, Germany, 2010, ISBN: 978-3642138843.

3. K. A. Tsokos, *Physics for the IB Diploma,* 5th ed., Cambridge University Press, Cambridge, UK, 2008, ISBN:
978-0521708203.

4. Urjart. (2008) Solar Cell: Basic Principle of Operation. [Online]. Available:
http://urjart.wordpress.com/2008/10/05/solar-cell-%E2%80%93-basic-principle-of-operation/

5. M. A. Green, "Solar cell fill factors: General graph and empirical expressions," *Solid-State Electronics*, vol. 24,
no. 8, pp. 788-789, 1981.

6. Zh. I. Alferov, “Heterostructures and their applications in optoelectronics”, *Akademiia Nauk SSSR*, vol. 7, pp.
28-40, 1976.

7. Stephen J. Fonash, *Solar Cell Device Physics,* 2nd Ed., Academic Press, Elsevier, Massachusetts, USA, 2010,
ISBN: 978-0123747747.

8. U. S. Department of Energy. (2011) Energy Basics. [Online]. Available:
http://www.eere.energy.gov/basics/renewable_energy/pv_cell_structures.html

9. Peter Wurfel, *Physics of Solar Cells: From Principles to New Concepts,* Wiley-VCH Verlag GmbH & Co.
KGaA, Weinheim, Germany, 2005, ISBN: 3-527-40428-7

10. L. J. A. Koster, E. C. P. Smits, V. D. Mihailetchi, and P. W. M. Blom, “Device model for the operation of
polymer/fullerene bulk heterojunction solar cells”, *Physical Review B*, vol. 72, pp. 085205-1 - 085205-9, 2005,
DOI: 10.1103/PhysRevB.72.085205

11. T. Tiedje, E. Yablonovitch, G. D. Cody, and B. G. Brooks, “Limiting efficiency of Silicon solar cells”, *IEEE*
Transactions on Electron Devices, vol. ED-31, pp. 711-716, 1984.

12. L.W. James, “III-V Compound heterojunction solar cells”, in *Proceedings of IEEE International Electron*
Devices Meeting, vol. 21, pp. 87-90, Washington, USA, 1975.

13. J.E. Sutherland, and J.R. Hauser, “Optimum bandgap of several III–V heterojunction solar cells”, *Solid-State*
Electronics, vol. 22, no. 1, pp. 3-5, 1979.

14. B. G. Streetman, and S. K. Banerjee, *Solid State Electronic Devices,* 6th Ed., Prentice-Hall Inc., New Jersey,
USA, 2006, ISBN: 978-8120330207.

15. M. A. Green, K. Emery, Y. Hishikawa, W. Warta, and E. D. Dunlop, “Solar cell efficiency tables (version 39)”,
Progress in Photovoltaics: Research and Applications, vol. 20, pp. 12-20, 2012.

16. F. Dimroth, “High-efficiency solar cells from III-V compound semiconductors”, *Physica Status Solidi (c),* vol.
3, no. 3, pp. 373-379, 2006.

17. B. Garcia, Jr., “Indium Gallium Nitride Multijunction Solar Cell Simulation Using Silvaco Atlas”, M. Sc.
Thesis, Naval Postgraduate School, Monterey, California, June 2007.

18. M. Meyer, and R.A. Metzger, “Flying high: The Commercial Satellite Industry Convert to Compound
Semiconductor Solar Cells”, Compound Semiconductor, vol. 2, no. 6, pp. 22-24, 1996.

19. J.J. Schermer, G.J. Bauhuis, P. Mulder, E.J. Haverkamp, J. van Deelen, A.T.J. van Niftrik, and P.K. Larsen,
“Photon confinement in high-efficiency, thin-film III–V solar cells obtained by epitaxial lift-off”, *Thin Solid*
Films, vol. 511, pp. 645 – 653, 2006.

20. T.V. Torchynska, and G.P. Polupan, “III-V material solar cells for space application”, *Semiconductor Physics,*
Quantum Electronics & Optoelectronics, vol. 5, no. 1, pp. 63-70, 2002.

21. A. Goetzberger, C. Heblinga, and H. Schockb, “Photovoltaic materials, history, status and outlook”, *Materials*
Science and Engineering: R: Reports, vol. 40, no. 1, pp. 1-46, 2003.

22. J. L. Gray and Michael McLennan. (2008) Adept. [Online]. Available: http://nanohub.org/resources/adept/

23. A. S. Brown, U. K. Mishra, J. A. Henige, and M. J. Delaney, Journal of Vacuum Science & Technology B, vol.
6, no. 2, pp. 678-681, 1988.

24. L. Ajili, G. Scalari, N. Hoyler, M. Giovannini, and J. Faist, "InGaAs–AlInAs/InP terahertz quantum cascade
laser", *Applied Physics Letters,* vol. 87, pp. 141107-1 - 141107-3, 2005, DOI: 10.1063/1.2081122

25. M. S. Leite, R. L. Woo, W. D. Hong, D. C. Law, and H. A. Atwater, "InAlAs epitaxial growth for wide band
gap solar cells" in *IEEE Proceedings of 37th Photovoltaic Specialists Conference,* pp. 780-783, Seattle, USA,
2011.

26. M. S. Leite, R. L. Woo, W. D. Hong, D. C. Law, and H. A. Atwater, "Wide-band-gap InAlAs solar cell for an
alternative multijunction approach", *Applied Physics Letters,* vol. 98, pp. 093502-1 - 093502-3, 2011, DOI:
10.1063/1.3531756

27. ECEn IMMERSE Web Team, Brigham Young University. (2009) Energy Gap in III-V Ternary
Semiconductors. [Online]. Available: http://www.cleanroom.byu.edu/EW_ternary.phtml

28. Ioffe Physical Technical Institute. (2005) NSM Archive - Physical Properties of Semiconductors. [Online].
Available: http://www.ioffe.ru/SVA/NSM/Semicond/

29. Harish Palaniappan. (2012) Solar Cells. [Online]. Available: http://solar_cells.tripod.com/notes_sel_1.html

30. Stuart Bowden. (2010) Energy of a Photon | pveducation.org. [Online]. Available:
http://www.pveducation.org/pvcdrom/properties-of-sunlight/energy-of-photon

31. J. G. Fossum, "Physical operation of back-surface-field silicon solar cells," *IEEE Transactions on Electron*
Devices, vol. 24, no. 4, pp. 322-325, Apr. 1977.

32. L. Knuuttila, K. Kainu, M. Sopanen, and H. Lipsanen, "In(Ga)As quantum dots on Ge substrate," *Journal of*
Materials Science: Materials in Electronics, vol. 14, no. 5, pp. 349-352, 2003.

33. Ming-Chun Tseng, Ray-Hua Horng, Fan-Lei Wu, Snin-Nan Lin, Hsin Her Yu, and Dong-Sing Wuu,

"Crystalline quality and photovoltaic performance of InGaAs solar cells grown on GaAs substrate with
large-misoriented angle," *Vacuum,* vol. 86, no. 7, pp. 843-847, Feb. 2012.

34. Md. Sharafat Hossain, Nowshad Amin, M. A. Matin, M. Mannir Aliyu, Takhir Razykov, and Kamaruzzaman
Sopian, "A numerical study on the prospects of high efficiency ultra thin ZnxCd1-xS/ CdTe solar cell,"
Chalcogenide Letters, vol. 8, no. 3, pp. 263-272, Mar. 2011.

35. Lin Aiguo, Ding Jianning, Yuan Ningyi, Wang Shubo, Cheng Guanggui, and Lu Chao, "Analysis of the p+/p
window layer of thin film solar cells by simulation," *Journal of Semiconductors,* vol. 33, no. 2, pp. 023002-1 -
023002-6 , 2012. DOI:10.1088/1674-4926/33/2/023002

36. C. Lee, H. Efstathiadis, J. E. Raynolds, and P. Haldar, "Two-dimensional Computer Modeling of Single
Junction a-Si:H Solar Cells", in IEEE *Proceedings of 34th Photovoltaic Specialists Conference,* pp. 1118-1122,
Philadelphia, USA, 2009.

37. S. Bothra, and J.M. Borrego, "Design of GaAs solar cells with low doped base," *Solar Cells,* vol. 28, no. 1, pp.
95-102, Jan. 1990.

38. N. Bouarissa, and M. Boucenna, "Band parameters for AlAs, InAs and their ternary mixed crystals", *Physica*
Scripta, vol. 79, pp. 015701-1 - 015701-7 , 2009, DOI: 10.1088/0031-8949/79/01/015701

39. K. H. Goetz, D. Bimberg, H. Jurgensen, J. Selders, A.V.Solomonov, G.F.Glinskii, and M. Razeghi, "Optical
and crystallographic properties and impurity incorporation of GaxIn1−xAs (0.44<x<0.49) grown by liquid phase
epitaxy, vapor phase epitaxy, and metal organic chemical vapor deposition", *Journal of Applied Physics,* vol.
54, no.8, pp.4543-4552, 1983.

40. J.W. Matthews, and A.E. Blakeslee, "Defects in epitaxial multilayers: I. Misfit dislocations", *Journal of Crystal*
Growth, vol. 27, pp. 118- 125, 1974.

41. H. J. Scheel, P. Capper, *Crystal Growth Technology: From Fundamentals and Simulation to Large-scale*

Production, p. 307, Wiley-VCH Verlag GmbH & Co. KGaA, Weinheim, Germany, 2008, ISBN: 978-
3527317622

42. E. Popova, J. Faure-Vincent, C. Tiusan, C. Bellouard, H. Fischer, M. Hehn, F. Montaigne, M. Alnot, S.
Andrieu, and A. Schuhl, "Epitaxial MgO layer for low-resistance and coupling-free magnetic tunnel junctions",
Applied Physics Letters, vol. 81, no. 6, pp. 1035-1037, 2002.

43. P. K. Nayak, G. G. Belmonte, A. Kahn, J. Bisquert, and D. Cahen, "Photovoltaic efficiency limits and material
disorder", *Energy and Environmental Science,* 2012, vol. 5, pp. 6022-6039, DOI: 10.1039/c2ee03178g

44. K. Van Nieuwenhuysen, F. Duerinckx, I. Kuzma, D. van Gestel, G. Beaucarne, J. Poortmans, "Progress in
epitaxial deposition on low-cost substrates for thin-film crystalline silicon solar cells at IMEC", *Journal of*
Crystal Growth, vol. 287, pp. 438–441, 2006.

45. P. P. Boix, M.M.Wienk, R. A. J. Janssen, and G.Garcia-Belmonte, "Open-Circuit Voltage Limitation in Low-
Bandgap Diketopyrrolopyrrole-Based Polymer Solar Cells Processed from Different Solvents", Journal of
Physical Chemistry C, vol. 115, pp. 15075–15080, 2011.

46. Q. Diduck, and M. Margala, "Ballistic deflection transistor and logic circuits based on same", U.S. Patent
7576353, Aug. 18, 2009.

47. E. W. Kiewra, S. J. Koester, D. K. Sadana, G. Shahldi, and Y. Sun, "Buried channel MOSFET using III-V
compound semiconductors and high k gate dielectrics", US Patent App. Pub. No. US2008/ 0296622 A1, Dec.
2008.

48. L. P. Sadwick, C. W. Kim, K. L. Tan, and D. C. Streit, "Schottky barrier heights of n-type and p-type
$Al_{0.48}Ga_{0.52}As$", *IEEE Electron Device Letters,* vol. 12, pp. 626-628, Nov. 1991.

49. A.W. Bett , F. Dimroth , G. Stollwerck, and O.V. Sulima, "III-V compounds for solar cell applications",
Applied Physics A, vol. 69, pp. 119–129, 1999, DOI: 10.1007/s003399900062

50. T. H. Glisson, J. R. Hauser, M. A. Littlejohn, and C. K. Williams, “Energy bandgap and lattice constant
contours of III-V quaternary alloys”, Journal of Electronic Materials, vol. 7, no. 1, pp. 1-16, 1978.